Development of a modified Mach–Zehnder interferometer for time and space density measurements for laser wakefield acceleration

Armando V. F. Zuffi
IPEN/CNEN
São Paulo, SP, Brazil
armandozuffi@gmail.com

Edison P. Maldonado
IEE – ITA
São José dos Campos, SP, Brazil
puigmald@gmail.com

Nilson D. Vieira Jr.
IPEN/CNEN
São Paulo, SP, Brazil
nilsondiasvieirajr@gmail.com

Ricardo E. Samad
IPEN/CNEN
São Paulo, SP, Brazil
resamad@gmail.com

2021 SBFoton International Optics and Photonics Conference (SBFoton IOPC) | 978-1-6654-1948-2/21/$31.00 ©2021 IEEE | DOI: 10.1109/SBFOTONIOPC50774.2021.9461961

***Abstract*—This work reports the development of a modified Mach–Zehnder interferometer aimed at determining the density of gas targets and laser generated plasmas, in time and space. This interferometer will compose our laboratory implementations for laser wakefield acceleration, allowing the characterizations of gas jet profiles generated by submillimeter nozzles. The technique also allows us to estimate the temporal evolution of the plasma density.**

Keywords—interferometry, gas density measurements, plasma density measurements, laser induced plasma, laser wakefield acceleration.

I. Introduction

Laser wakefield acceleration (LWFA) has been growing rapidly in the scientific community as a new concept for the next generation of compact particle accelerators [1, 2]. Due to the formation of acceleration gradients over 100 GV/m, compared to those currently limited to ~100 MV/m in conventional RF accelerators [3], LWFA reduces the dimensions to a laboratory scale, with proportional decrease in costs and complexity. This kind of acceleration is usually achieved in gaseous target where high intensity laser pulses create a plasma and a wake that moves with almost the speed of light, stimulating the creation of a longitudinal electric field capable of accelerating electrons (wakefield) [4] up to GeV in a few centimeters [5]. The simplicity of LWFA is driving the widespread of traditional applications [6], like the production of isotopes for medicine [7, 8], and high resolution x-ray imaging [9], among other applications.

The onset of the LWFA requires the control of the laser parameters (pulse energy and duration, beam area and focusing conditions) and the plasma density, size and duration. The plasma density depends on the gas type (monoatomic, diatomic, etc) its density and ionization energies, and its profile. The control of the parameters and conditions of the LWFA requires a series of diagnostic systems to characterize and improve the electron beam generation and its parameters (energy, divergence, charge). A large part of the effort to have a LWFA running, is devoted to diagnostics, which prevent operation if not available [10]. Among those, several optical techniques are used to characterize the gas jet, plasma, wakefield and the electron beam [11], including fluorescence [11], spectroscopy [12], interferometry [13] and schlieren imaging [14], among others [11].

Interferometry is a very precise technique capable of measuring very small optical path differences and therefore suitable for measuring density variations in gas targets, excited plasmas and wakefields [15]. From an interferogram, the phase-shift accumulated by a laser beam propagating through a gas jet or plasma can be extracted, and consequently, their density distribution can be determined. While a continuously flowing gas target can be diagnosed by CW interferometry, to analyze a laser excited plasma pump-probe techniques [10] are needed due to the short plasma formation time and excited ions fast decay, which would make the signal fade out in CW techniques due to the exceedingly small duty-cycle.

In our laboratory, we are working to implement a laser electron acceleration infrastructure [16, 17]. For that, we are focusing efforts on the development of a modified Mach–Zehnder interferometer capable of diagnosing transient phenomena in gas targets and laser created plasmas. The development and implementation of this interferometer will provide useful information about the plasma conditions suitable for the LWFA process.

II. Experimental Setup

The Ti:sapphire CPA laser system used for pump-probe interferometry experiments (Femtolasers Femtopower Compact Pro HR/HP) generates 25 fs (FWHM) pulses centered at 785 nm with 40 nm of bandwidth (FWHM), up to 650 μJ, at 4 kHz repetition rate, producing a laser beam with an M^2 factor of 1.5. A beam sampler extracts a fraction of the pulses energy, which are sent through a delay line and are focused in a BBO crystal to generate second harmonic pulses at 395 nm. The second harmonic is collimated into a ~5 mm diameter beam, and these synchronized blue pulses are sent to the modified Mach–Zehnder interferometer to characterize the gas jets and the plasma formed by the fundamental pulses. Second harmonic pulses were chosen to be used in the interferometer due to the higher fringes resolution when compared to the fundamental wavelength, and also to minimize the scattered laser background on the CCD by the use of filters.

The modified Mach–Zehnder interferometer setup is being employed in the characterization of homemade submillimetric de Laval nozzles through the analysis of the generated gas jets profiles and their densities. Moreover, the modified setup can perform time-resolved measurements of the plasma formed by the fundamental pulses, and consequently, the wakefield channel formation.

Fig. 1.a presents a scheme of the modified Mach–Zehnder interferometer. The polarized 395 nm probe beam pulse enters the interferometer and is divided by a beamsplitter (BS1) into a reference (reflected) and a diagnostic (transmitted) beams. The diagnostic beam propagates through the gas jet and/or

This work was supported by FAPESP, SAE and CNPq.

978-0-7381-2418-6/21/$31.00 ©2021 IEEE

plasma, positioned in the pump beam focus (in red). The phase-shift accumulated in this arm can be obtained by overlapping it with the reference pulse, after their recombination in the BS2 beamsplitter. The temporal overlap between the reference and the diagnostic pulses is attained by adjusting the reference pulse delay using a translation stage supporting 2 mirrors in a roof configuration. The 15 cm convergent lens L produces a 3× magnified interferogram of the target at the CCD. The BS2 beamsplitter also directs the two beams to a spectrometer, creating a spectral fringe pattern (Fig. 1.b) when the interferometer two arms have the same optical length within the pulses coherence length. These spectral fringes are easier to find than the spatial interference ones, and they are used to set the two arms with the same optical length; once this "zero-delay" position is found, the interference fringes can be seen in the CCD (Fig. 1.c), and small adjustments in the reference arm mirrors define the fringes direction and spatial frequency. Furthermore, we have implemented a small vacuum chamber with Brewster windows [16], which can be fitted to the nozzle, allowing the study of its performance in vacuum when applying a backing pressure up to 50 bar.

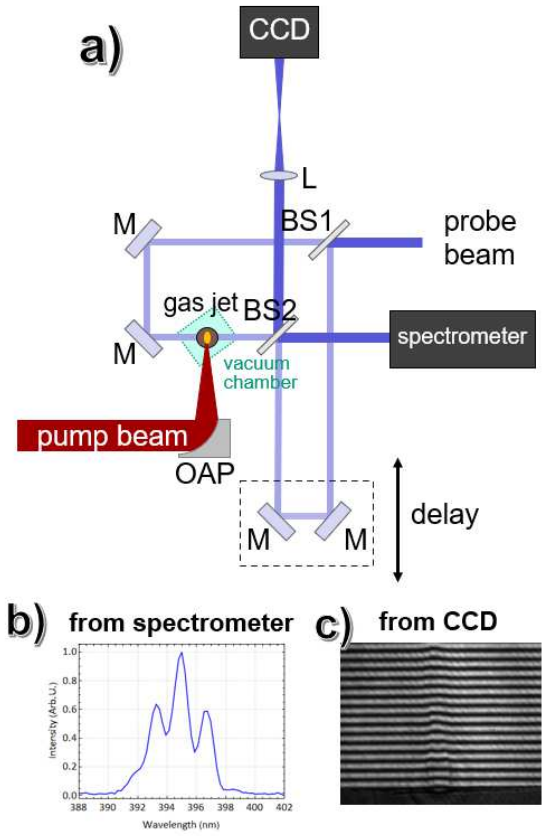

Fig. 1. (a) Modified Mach–Zehnder interferometer setup. Probe beam in blue and pump beam in red, OAP = off-axis parabolic mirror, BS = beamsplitter, M = mirror, L = lens. (b) Spectral fringes. (c) Spatial interferogram.

The phase-shift caused by the target (gas jet or plasma) is visualized from the bending of the interferogram fringes [18]. The common way to retrieve the accumulated phase-map from the 2D interferogram consists of: (1) obtaining an interferogram of the background (*bg*) and another of the background+target (*bg+t*); (2) transforming both interferograms to the frequency domain by 2D Fourier transforms; (3) applying a filter over the region that contains the target phase-shift information [19] in both frequency domain maps; (4) performing an inverse Fourier transform to the filtered 2D spectra, generating *bg* and *bg+t* phase-shift maps with discontinuities, and applying a 1D unwrapping algorithm to obtain continuous *bg* and *bg+t* phase shift maps; (5) subtracting the *bg* phase-shift map from the *bg+t* map, to obtain the target phase-shift map [19, 20].

The density distribution of the gas jet or plasma can be obtained from the phase-shift map. In the case of a cylindrically symmetric gas jet, the integrated information along one axis is sufficient to reconstruct the 3D density profile using inversion techniques such as the Abel inversion method [20], which is generally used considering that imperfections in the cylindrical symmetry of real targets are second order corrections.

III. Results

A. Gas jet characterization

Fig. 2.a shows a background (*bg*) interferogram obtained inside the vacuum chamber (~100 mbar pressure), and Fig. 2.b presents the interferogram of the gas jet generated by a home-made nozzle with 50 bar of N_2 backing pressure inside the same chamber. A high-pressure region can be seen immediately above the nozzle exit (fringes shift in the lower part of Fig. 2.b); the rapid gas expansion in the vacuum chamber and the consequent density drop along the gas propagation axis gradually decrease the fringes shift.

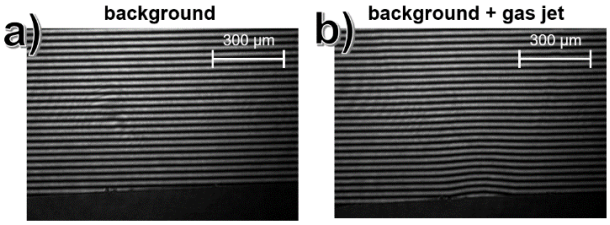

Fig. 2. Interferograms obtained inside the vacuum chamber for: (a) background (~100 mb), and (b) gas jet with 50 bar N_2 backing pressure.

In order to determine the gas jet density profile from interferograms, we developed a phase retrieval algorithm on the Mathematica® Software (Wolfram Research). Fig. 3 presents the phase-shift map obtained from the interferograms shown in Fig. 2, using the method described in the introduction, and shows the gas jet geometry. Despite some noise impairs the final phase-shift map, a clear visualization of the gas jet expansion is depicted indicating the adequacy of the interferometer and the algorithm used. Moreover, we are working on computational techniques to remove this noise and improving the experimental setup isolation to reduce mechanical instabilities and unwanted diffractions in the interferograms.

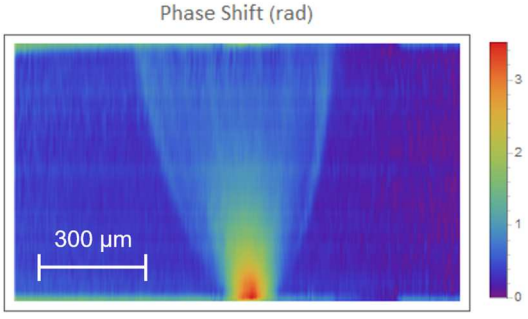

Fig. 3. Phase-shift map of the gas flow into ~100 mbar background pressure and 50 bar of N_2 backing pressure.

From that phase-shift map, we can estimate the spatial refractive index distribution by:

$$n = 1 + \Delta\phi\, \lambda_{probe}/(2\pi\, l), \quad (1)$$

where $\Delta\phi$ is the measured phase-shift, $\lambda_{probe} = 395$ nm is the interferometer wavelength and l is the gas jet diameter, which was estimated from the phase map to be 190 µm assuming a cylindrical symmetry of the jet, and a background refractive index of 1 (ideal vacuum). From the refractive index 2D map and eq. (1) we also can estimate the gas molecular density distribution using the simple expression of the Lorentz-Lorenz relation [21, 22]:

$$N_g = 3/(4\pi\alpha)\times(n^2 - 1)/(n^3 + 2), \quad (2)$$

where α is the molecular polarizability, which for N_2 is 1.710 Å^3[23]. Fig. 4 shows the radial density profile distribution for heights of 0, 100, 200, 400, and 600 µm above the nozzle exit. Immediately at the nozzle exit this density is 1.55×10^{20} molecules/cm^3, a high density in the range needed to carry out electron acceleration experiments in the self-modulated LWFA (SM-LWFA) regime [24, 25], as we intend to perform in our lab.

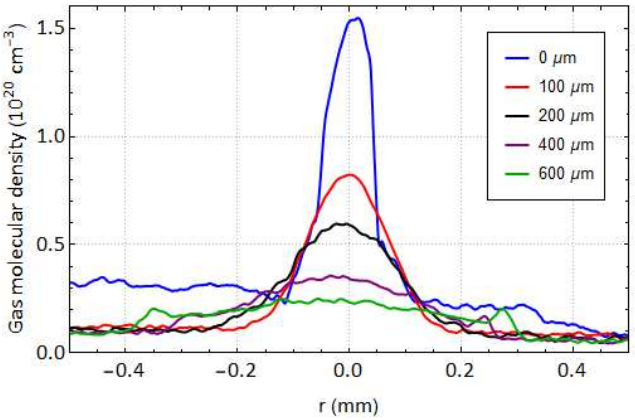

Fig. 4. Radial density profile distribution at 0, 100, 200, 400, and 600 µm above the nozzle exit, for the jet shown in Fig. 3.

B. *Plasma characterization*

Fig. 5 shows a 395 nm interferogram of a plasma formed in atmosphere by the 785 nm, 250 µJ, 25 fs laser pulses in a beam with $M^2\approx1.5$ focused by a 50 mm off-axis parabolic mirror [16], to an intensity of 1.5×10^{16} W/cm^2, corresponding to a peak intensity of 3.0×10^{16} W/cm^2 . The plasma presence is evidenced by the fringe shift as well as a brightness increase due to its emission. From this interferogram, the plasma induced phase-shift in the probe beam can be retrieved.

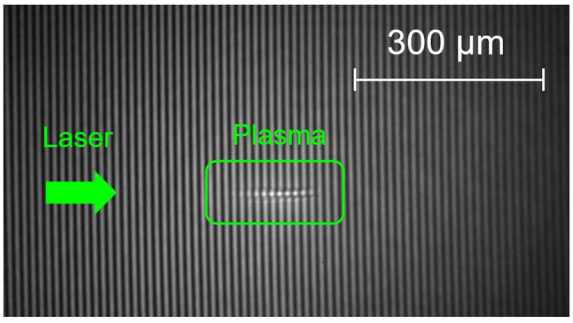

Fig. 5. Interferogram of a plasma formed in atmosphere (circled in green). The pump laser propagation direction is indicated by the green arrow.

Fig. 6 presents three density maps of the plasma obtained at different times after its formation (150 ps, 300 ps and 450 ps), allowing the study of the plasma temporal and spatial evolution.

Those densities were estimated using equation (1) and the plasma refractive index given by [26]:

$$n = 1 - \omega_p^2 / \omega_0^2 \approx 1 - N_e\, e^2\lambda_0^2 /(8\pi^2 c^2\, m_e\, \varepsilon_0), \quad (3)$$

where N_e is the electrons density in the plasma, λ_0 is the pump pulse wavelength, e and m_e are the electron charge and mass, c is the speed of light in vacuum, ε_0 is the vacuum permittivity, ω_p^2 and ω_0 are, respectively, the plasma and pump laser frequencies.

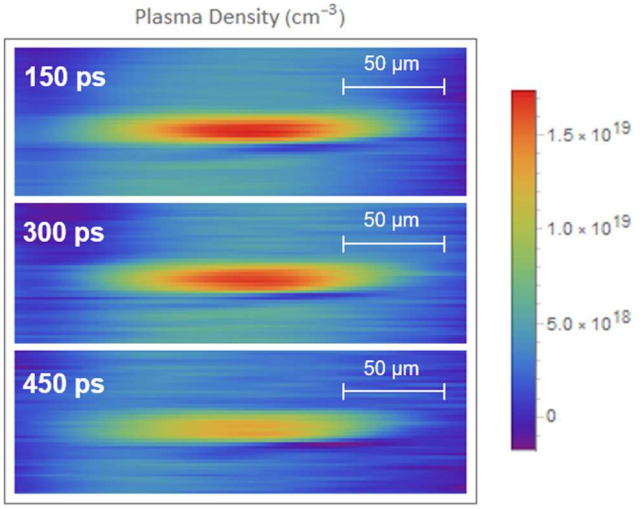

Fig. 6. Density maps of the plasma in the atmosphere for different times after its formation.

Although these maps present noise, we can observe that the plasma dimensions and density decrease with time, demonstrating the interferometer and technique efficiencies. Furthermore, we could estimate the plasma temporal evolution up to hundreds of ps, as exemplified by the plasma peak density decrease from about 1.8×10^{19} to 1.3×10^{19} electrons/cm^3 over time, as presented in Fig. 7.

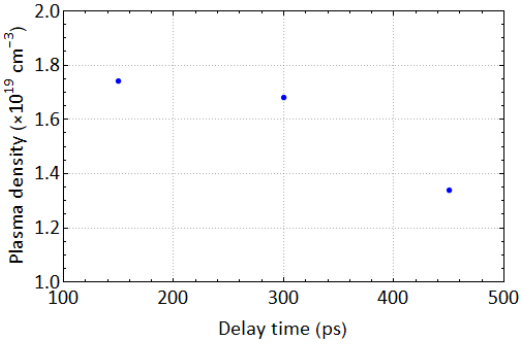

Fig. 7. Temporal evolution of the plasma peak density extracted from the data shown in Fig. 6.

To verify if the measured plasma densities are in accordance with the theoretical predictions, we assumed that the air is composed only of nitrogen molecules, which is 5 times ionized by the 3.0×10^{16} W/cm^2 peak intensity attained [27], according to Table I:

TABLE I. NITROGEN IONIZATION THRESHOLD INTENSITIES

Ionization state	*Ionization energy (eV)*	*Laser intensity (W/cm^2)*
+1	14.53	1.8×10^{14}
+2	29.60	7.7×10^{14}
+3	47.45	2.3×10^{15}
+4	77.48	9.0×10^{15}
+5	97.89	1.5×10^{16}
+6	552.1	1.0×10^{19}
+7	667.1	1.6×10^{19}

Considering an atmospheric pressure density of $\sim2.5\times10^{19}$ molecules/cm^3 and only the pulses peak intensity, we should have obtained a plasma electron peak density of $\sim2.5\times10^{20}$ electrons/cm^3 for an ideal case, in contrast with the maximum density of 1.8×10^{19} shown in Fig. 6. This discrepancy may have three main causes: firstly, we did not consider the ionization profile due to the intensity distribution, which would decrease the total number of free electrons generated; also, the measurement was done 100 ps after the plasma formation, providing time for recombination that decreased the plasma electrons density; in addition, the electron density obtained from the phase-shift maps did not consider the transversal electrons ionization profile, assuming it is constant, and this should be corrected by an Abel transform [28], which considers a cylindrical symmetry and radial profile, and should increase the peak density by a 2-3 factor. We are working to better understand this discrepancy.

IV. Conclusions

In this work, we developed and built a new time-resolved Mach–Zehnder interferometer to diagnose gas jet targets and generated plasmas in laser wakefield acceleration. The use of a spectrometer proved to be an important tool to find the pulses temporal overlap, readily providing the correct arm length to create spatial interferograms on the CCD. We showed that the interferometer can be used to characterize a gas jet expansion inside a vacuum chamber, obtaining phase-shift maps that return its geometry and density, as well as the time evolution of the formed plasma, also allowing the estimation of its density.

Acknowledgment

The authors would like to acknowledge the financial support from FAPESP, SAE and CNPq, and A. V. F. Zuffi thanks CNPq for a scholarship.

References

[1] T. Katsouleas, "Accelerator physics - Electrons hang ten on laser wake," Nature, vol. 431, pp. 515-516, 2004.

[2] T. Tajima, K. Nakajima, and G. Mourou, "Laser acceleration," Rivista Del Nuovo Cimento, vol. 40, pp. 33-102, 2017.

[3] V. Malka, "Plasma Wake Accelerators: Introduction and Historical Overview," Cern Yellow Rep., vol. vol. CERN-2016-, pp. 1–28, 2016.

[4] E. Esarey, C. B. Schroeder, and W. P. Leemans, "Physics of laser-driven plasma-based electron accelerators," Rev. Mod. Phys., vol. 81, pp. 1229-1285, 2009.

[5] W. P. Leemans, "GeV electron beams from a centimetre-scale accelerator," Nat. Phys., vol. 2, pp. 696-699, 2006.

[6] F. Albert, "Laser Wakefield Accelerators: Next-Generation Light Sources," Optics and Photonics News, 29(January 2018), pp. 42-49, 2018.

[7] K. Nemoto, "Laser-triggered ion acceleration and table top isotope production," Appl. Phys. Lett., vol. 78, pp. 595-597, 2001.

[8] I. Spencer, "Laser generation of proton beams for the production of short-lived positron emitting radioisotopes," Nucl Instrum Meth B, vol. 183, pp. 449-458, 2001.

[9] L. Labate, "Toward an effective use of laser-driven very high energy electrons for radiotherapy: Feasibility assessment of multi-field and intensity modulation irradiation schemes," Sci. Rep., vol. 10, 2020.

[10] M. C. Downer, R. Zgadzaj, A. Debus, U. Schramm, and M. C. Kaluza, "Diagnostics for plasma-based electron accelerators," Rev. Mod. Phys., vol. 90, 2018.

[11] A. J. Goers, "Multi-MeV Electron Acceleration by Subterawatt Laser Pulses," Phys. Rev. Lett., vol. 115, 2015.

[12] S. Shiraishi, "Laser red shifting based characterization of wakefield excitation in a laser-plasma accelerator," Phys. Plasmas, vol. 20, 2013.

[13] G. Costa, "Characterization of self-injected electron beams from LWFA experiments at SPARC_LAB," Nucl Instrum Meth A, vol. 909, pp. 118-122, 2018.

[14] G. S. Settles, Schlieren and shadowgraph techniques : visualizing phenomena in transparent media. Berlin ; New York: Springer, 2001.

[15] F. Brandi, and L. A. Gizzi, "Optical diagnostics for density measurement in high-quality laser-plasma electron accelerators," High Power Laser Science and Engineering, vol. 7, 2019.

[16] R. E. Samad, A. V. F. Zuffi, E. P. Maldonado, and N. D. Vieira, "Development and Optical Characterization of Supersonic Gas Targets for High-Intensity Laser Plasma Studies," presented at the 2018 SBFoton International Optics and Photonics Conference (SBFoton IOPC), Campinas, Brazil 2018.

[17] N. D. Vieira, R. E. Samad, and E. P. Maldonado, "Compact Laser Accelerators Towards Medical Applications - perspectives for a Brazilian Program," 2019 Sbfoton International Optics and Photonics Conference (Sbfoton Iopc), 2019.

[18] A. K. Arunachalam, "Investigation of laser-plasma interactions at near-critical densities," University of Jena, 2017

[19] J. P. Couperus, "Tomographic characterisation of gas-jet targets for laser wakefield acceleration," Nucl Instrum Meth A, vol. 830, pp. 504-509, 2016.

[20] V. Malka, "Characterization of neutral density profile in a wide range of pressure of cylindrical pulsed gas jets," Rev. Sci. Instrum., vol. 71, pp. 2329-2333, 2000.

[21] H. A. Lorentz, "Über die Beziehungzwischen der Fortpflanzungsgeschwindigkeit des Lichtes derKörperdichte," Ann. Phys. 9, pp. 641-665, 1880.

[22] L. Lorenz, "Über die Refractionsconstante," Ann. Phys. 11, pp. 70-103, 1880.

[23] T. N. Olney, N. M. Cann, G. Cooper, and C. E. Brion, "Absolute scale determination for photoabsorption spectra and the calculation of molecular properties using dipole sum rules," Chem Phys, vol. 223, pp. 59-98, 1997.

[24] N. Lemos, "Self-modulated laser wakefield accelerators as x-ray sources," Plasma Phys Contr F, vol. 58, 2016.

[25] A. T. J. Krall, E. Esarey and P. Sprangle, "Self-modulated-laser wakefield acceleration," in *International Conference on Particle Accelerators*, 1993, pp. 2629-2631.

[26] J. T. Verdeyen, and J. B. Gerardo, "Application of Laser to Plasma Refractive Index Determination," Ann. NY Acad. Sci., vol. 122, pp. 676-684, 1965.

[27] H. A. Bethe, and E. E. Salpeter, Quantum Mechanics of One- and Two-Electron Atoms. Boston, MA: Springer US,, 1977.

[28] S. Shi, K. Finch, Y. She, and G. Gamez, "Development of Abel's Inversion Method to Extract Radially Resolved Optical Emission Maps from Spectral Data Cubes Collected via Push-Broom Hyperspectral Imaging with Sub-pixel Shifting Sampling," J. Anal. At. Spectrom., 2019.